NANO LETTERS

LETTER

pubs.acs.org/NanoLett

Air Stable, Photosensitive, Phase Pure Iron Pyrite Nanocrystal Thin Films for Photovoltaic Application

Yu Bi,[†,‡] Yongbo Yuan,[†,§] Christopher L. Exstrom,[§,∥] Scott A. Darveau,[§,∥] and Jinsong Huang*[,†,§]

[†]Department of Mechanical and Materials Engineering, University of Nebraska—Lincoln, Lincoln, Nebraska 68588, United States

[‡]Key Laboratory of Semiconductor Materials Science, Institute of Semiconductors, Chinese Academy of Sciences, Beijing 100083, People's Republic of China

[§]Nebraska Center for Materials and Nanoscience, University of Nebraska—Lincoln, Lincoln, Nebraska 68583-0298, United States

[∥]Department of Chemistry, University of Nebraska at Kearney, Kearney, Nebraska 68849-1150, United States

Supporting Information

ABSTRACT: Iron pyrite (FeS_2) is a naturally abundant and nontoxic photovoltaic material that can potentially make devices as efficient as silicon-based ones; however existing iron pyrite photovoltaic devices contain thermodynamically unstable FeS_2 film surfaces that lead to low open circuit voltages. We report the rational synthesis of phase pure, highly crystalline cubic FeS_2 nanocrystals (NCs) using a trioctylphosphine oxide (TOPO) assisted hot-injection method. The synthesized pyrite NC films have excellent air stability over one year. In contrast, obvious surface decomposition was observed on the surface of FeS_2 NCs synthesized without TOPO. A high carrier mobility of 80 $cm^2/(V\ s)$ and a strong photoconductivity were observed for the first time for pyrite films at room temperature. Our results indicate that TOPO passivates both iron and sulfur atoms on FeS_2 NC surfaces, efficiently inhibiting surface decomposition.

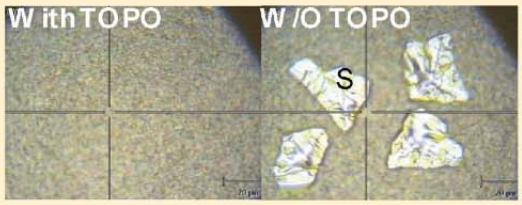

KEYWORDS: Nanocrystals, iron pyrite, photovoltaic, photoconductive

Iron pyrite is a very attractive next-generation photovoltaic (PV) material that is abundant in nature and nontoxic. Its high natural abundance translates to an estimated 0.000002 ¢/W material extraction cost, which ranks FeS_2 highest in regards to the material availability among 23 existing semiconductor material systems that potentially lead to substantially lower costs than silicon.[1] A pyrite cell with only 4% efficiency could be as cost effective as a similar single crystalline silicon solar cell reporting 20% efficiency.[1,2] The very high absorption coefficient ($\sim 5 \times 10^5\ cm^{-1}$) and a suitable energy band gap ($E_g \approx 0.95$ eV) for photovoltaic energy conversion are particular advantages of pyrite. The estimated highest attainable efficiency of pyrite PV films is as high as that for single crystal silicon.[3] Iron pyrite has the potential to become an important material for large scale manufacturing of thin film PV modules in which the elemental constituents are abundant and nontoxic.[4]

Despite the huge promise that iron pyrite holds, no efficient iron pyrite-based PV devices currently exist. The highest efficiency (2.8%) has been obtained in a photoelectrochemical cell.[4−8] The limiting factor for a high efficiency is the high dark current which leads to small open circuit voltages, less than 0.2 V, that are caused by iron pyrite phase impurities and, more importantly, large density surface states.[5] The large density surface states originate from thermodynamically unstable particle surfaces that are terminated with sulfur dimers.[9] The sulfur dimers tend to segregate to the surface and cause vanishing of the hybridized band, at the top of the Fe layer, making the surface effectively similar to a 1S termination. An iron monosulfide (FeS) structure is formed on the surface of the pyrite crystals. This results in a large density of defect states in the middle of pyrite band gap that reduced the band gap at the surface to nearly zero.

Several methods for the synthesis of pyrite thin films have been reported, including sulfurization of iron, MOCVD deposition, and the sintering of colloidal NCs prepared solvothermally.[10−12] However, photoresponse (or photoconductivity) has rarely been observed in these films at room temperature. This may be caused by significant charge recombination at interface surfaces.[13,14] The combination of low-cost solution preparation and processing methods with a low-cost absorber material has the potential to produce very low cost iron pyrite solar cell devices.[12,15] It remains to be seen whether these synthesized pyrite NCs would produce the thin film with stable surface and correlated desired electronic properties for PV application.

In this paper, we report the synthesis of pyrite NCs using a surfactant assisted hot-injection method that yields phase pure, highly crystalline, surface stable NCs. The NC film formed from a modified dip-coating method shows an excellent absorption coefficient of $2 \times 10^5\ cm^{-1}$ and high carrier mobility of

Received: August 21, 2011
Revised: September 20, 2011
Published: October 12, 2011

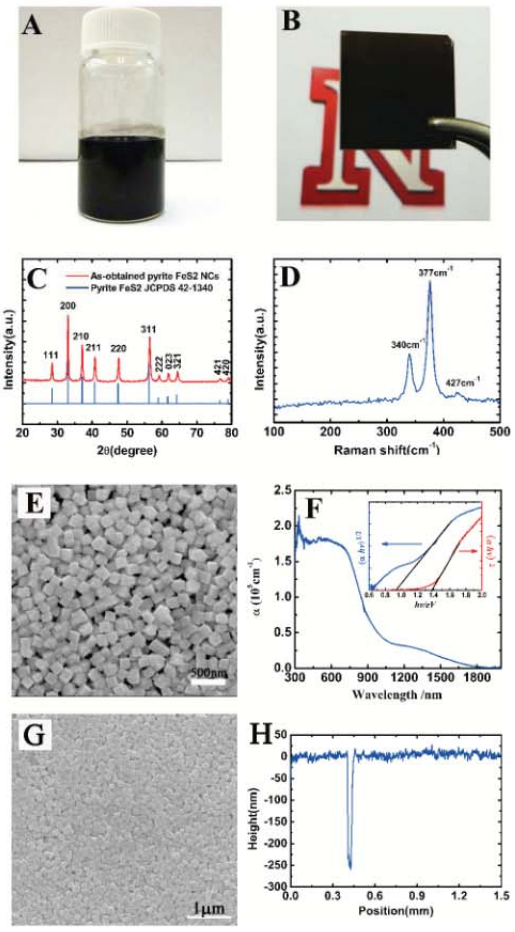

Figure 1. (A) Photograph of as-obtained pyrite FeS_2 NCs solution in chloroform. (B) Photograph of as-obtained pyrite FeS_2 NC film. (C) XRD pattern, (D) Raman spectroscopy, and (E) SEM image of as-obtained NCs by drop casting. (F) Absorption spectra of as-obtained NC film (insert is plots of $(\alpha h\nu)^n$ vs $h\nu$ $n = {}^1/_2$, 2). (G) SEM image of pyrite NC film formed by dip coating using NCs with a size of 60 nm (H) and its surface profile with a scratch for thickness measurement.

80 $cm^2/(V\ s)$. Moreover, excellent air stability of the NC film over 1 year was obtained, and obvious photoconductivity at room temperature was observed for the first time.

The pyrite FeS_2 NCs were prepared by using the coordinating solvent oleylamine (OLA) combined with TOPO to form a soluble Fe precursor species at 170 °C. Sulfur stock solution in OLA was then injected and the reaction proceeded for 2 h at 220 °C. The reactions were systematically optimized, resulting in the successful synthesis of pure phase and monodisperse cubic iron pyrite NCs without the need for a size-selecting process.

Figure 1 shows a photograph of iron pyrite NC ink and film, XRD pattern, Raman spectrum, SEM image, and absorption spectrum of NC film. The XRD diffraction peaks (Figure 1C) can be indexed as a pure pyrite cubic phase of FeS_2 (JCPDS no. 42-130), and no obvious impurity peaks were observed. The sharp peaks in the XRD pattern indicate the excellent crystallinity of the as-obtained FeS_2 NCs. Raman spectroscopy was applied to further confirm the pure phase of pyrite FeS_2 NCs due to its capability to distinguish iron sulfide phases[16] (FeS, Fe_3S_4, FeS_2) and its lower impurity detection limits than XRD. Raman peaks for FeS (210 and 280 cm^{-1})[29] were not observed here, indicating the high phase purity of our NCs. Figure 1E shows Raman peaks at 339, 378, and 425 cm^{-1} for the as-obtained NCs, that match well with the reported values for pyrite FeS_2.[17,18] The phase purity of the pyrite was further verified by very sensitive magnetic measurements. Iron ions in $Fe_{1-x}S$ and FeS_2 have a high and low spin state, respectively, with a huge difference of 8 orders of magnitude. The synthesized pyrite NCs show no magnetism signal to the detection limit of the superconducting quantum interference device (SQUID), demonstrating $Fe_{1-x}S$ impurity level is below parts per million (ppm).

A typical SEM image in Figure 1E shows the as-obtained FeS_2 NCs synthesized with TOPO/OA as its coordinating solvent as having cubic shape and good uniformity. The size of the NCs can be controlled between 60 and 200 nm by increasing the amount of TOPO (see Figure S1 in the Supporting Information). Relatively large sized NCs that correspond to the proper film thickness for PV applications were targeted in this work because the quantum confinement effect is not needed for band gap control. Typically a large crystalline grain size in PV films is preferred for a large carrier diffusion length to be matched with the light absorption length. Smaller size NCs can form a smooth and compact film. However the large amount of boundaries in the film made of the small size pyrite NCs will inevitably scatter carrier and reduce carrier diffusion length. We were able to get smooth pyrite NC films with surface roughnesses of ±25 nm using a modified dip coating method (Figure 1H). A pyrite film thickness around 0.4 μm is needed for the efficient absorption of solar radiation. Therefore, such small roughness should be within the tolerance for thin film PV applications.

Figure 1F shows the absorption spectra of as-obtained FeS_2 NC film made by the dip-coating method. With a high absorption efficiency (approximately 2×10^5 cm^{-1}) for NC film throughout visible and near-infrared spectral regions, the pyrite NC film is clearly an excellent solar absorber material. The band gap of pyrite, an important parameter for solar cell applications, is still under debate[19,20] because it has been difficult to obtain high-purity crystalline pyrite materials.[2] Due to the excellent uniformity and crystallinity of the pyrite NCs we have, the indirect and direct optical band gaps of FeS_2 NCs were clearly determined by the absorption spectra[21,22] to be 0.93 and 1.38 eV, respectively. It should be noted that light absorption below the band gap can be induced by light scattering during the measurement.

Stable well-dispersed NCs in chloroform solution were obtained after isolation without any post-treatment, the solution (Figure 1A) is stable for 2 months without obvious particle aggregation or sedimentation. The particle size (100 nm) is larger than most of the other reported colloidal NCs such as PbS[23,24] and CdSe,[25−27] indicating that there are suitable ligands on the surface of FeS_2 NCs. These ligands appear to play a dominating role in surface passivation of pyrite FeS_2 NCs.

It has been controversial whether the formation of iron pyrite goes through the intermediate product of FeS.[28] In order to understand the reaction process of forming pyrite NCs, the morphology and composition of the reaction products at the initial stage of the synthesis were studied by XRD, Raman spectra, and

dx.doi.org/10.1021/nl202902z |Nano Lett. 2011, 11, 4953–4957

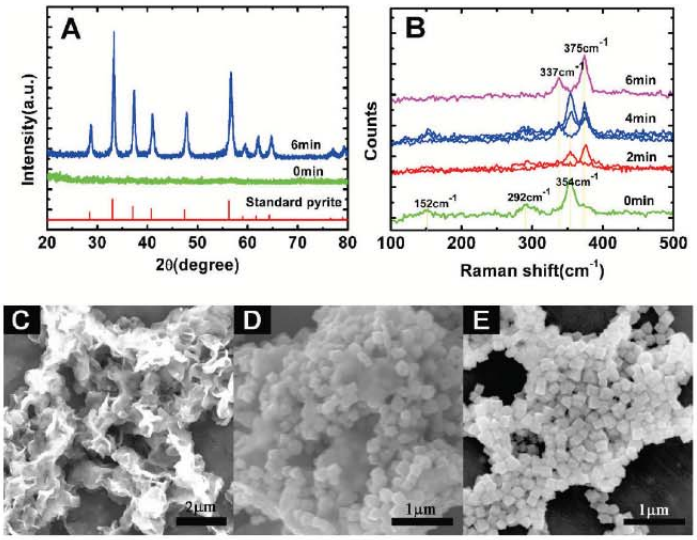

Figure 2. (A) XRD pattern and (B) Raman spectra of as-obtained product from different reaction time after injecting sulfur stock solution into the Fe precursor which yielded with TOPO. (C−E) SEM images of the reaction process from amorphous $Fe_{1-x}S$ to cubic FeS_2 during the reaction, 2, 4, and 6 min after sulfur injection. There were multiple lines for 2 and 4 min corresponding to multiple scanning at different locations.

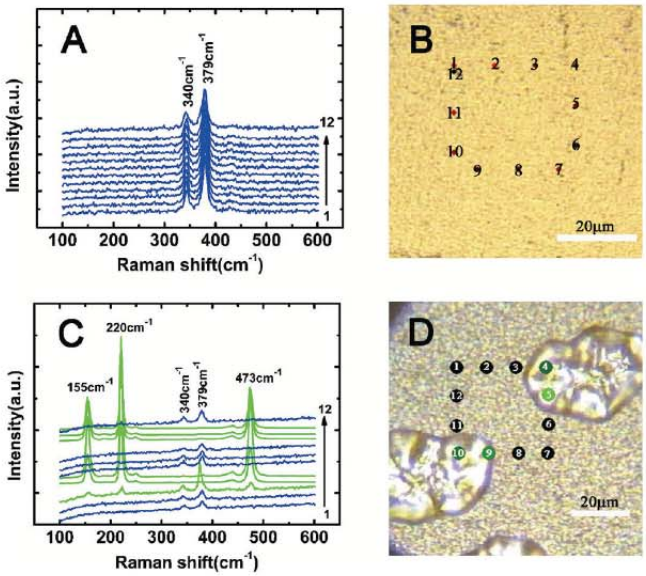

Figure 3. Typical Raman mapping of pyrite NC film (A) made with TOPO in the reaction mixture. (B) The corresponding mapping picture after exposure in air for 1 year. (C) Film made without TOPO. (D) Its corresponding mapping picture after exposure in air for 3 months.

SEM, and the results are shown in Figure 2. Panels A and B of Figure 2 indicate that there is no FeS phase (absence of Raman peaks at 210 and 280 cm^{-1})[29] observed during the reaction, but amorphous $Fe_{1-x}S$ (Raman peaks at 152, 292, and 354 cm^{-1}) is formed initially after the sulfur injection. The transformation from this amorphous intermediate to pyrite FeS_2 NCs only takes 6 min. During this time, the reaction product is a mixture of amorphous phase and pyrite FeS_2. SEM images (Figure 2C E) directly show the process of pyrite cubic NC formation, in which the cubic NCs grow out of the amorphous matrix over time.

dx.doi.org/10.1021/nl202902z |*Nano Lett.* 2011, 11, 4953–4957

It should be noted that the reaction process is essentially the same even without TOPO, as demonstrated by similar study shown in Figure S2 in the Supporting Information.

The stability of nanomaterials in air is another important factor for the development of NC photovoltaics. The stability issue is an especially important concern for pyrite FeS_2 NCs because its surface structure is not stable thermodynamically.[9] FeS_2 units on particle surfaces are susceptible to oxidation and can easily decompose. The large surface areas of NCs can accelerate the oxidization process dramatically. Decomposition results in metallic FeS and sulfur (S) surface layers on the NCs semiconducting properties are lost. In our studies, we found that pyrite NC films made with TOPO in the reaction mixture are stable in air for at least 1 year according to Raman spectroscopy (Figure 3) and XRD studies (Figure S3, Supporting Information).

As shown in panels A and B of Figure 3, we randomly chose spots on different NC film samples after storage in air for 1 year to perform Raman spectroscopy. There was no observation of any FeS or S Raman peaks. Visually, the pyrite film looks no different after exposure to air for 1 year. As a control experiment, pure pyrite NCs was prepared under the same reaction conditions except that TOPO was absent. After exposure to air for 3 months, the pyrite NC films were oxidized as indicated by FeS and S Raman peaks (Figure 3C) and XRD signals (Figure S3, Supporting Information). Visually, there is obvious sulfur segregation from the surface of iron pyrite film (Figure 3D).

Pyrite NC stability improves dramatically when prepared with TOPO in the reaction mixture. We speculate that TOPO participates in a surface passivation mechanism that could occur as shown in Scheme 1. Usually, in a TOPO/OLA mixture, TOPO will preferentially bind to Fe because phosphine oxides are slightly stronger bases than amines .[30] Phosphine oxide coordination can occur only through an oxygen atom,[31] while the phosphorus atom will coordinate sulfur due to attractive charge interactions. Therefore, TOPO will to coordinate to FeS_2 NCs and form stable surface structures that inhibit the segregation of sulfur dimers on the pyrite NC surfaces. As a result, both Fe and S surface sites are passivated. For pyrite NCs synthesized without TOPO in the reaction mixture, the only coordinating solvent is OLA which coordinates to iron through a nitrogen atom. Only Fe sites become passivated, leaving S dangling bonds available to react with O_2. This is consistent with the observation that sulfur segregates from the pyrite NC films as showed in Figure 3C,D.

Scheme 1. The speculated Surface Passivation Mechanism of TOPO to FeS_2 Surfaces

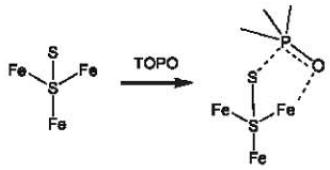

The electric properties of the dip-coated pyrite NC films were measured and evaluated for PV applications. The product of the mobility (μ) and carrier lifetime (τ) is the most important parameter to evaluate the candidacy of any PV material because it determines the carrier diffusion length, i.e., the maximum thickness of the active film. A large $\mu\tau$ is preferred so that a relatively thick film can be applied to absorb the most of the solar illumination. The measured Hall effect mobility of the pristine pyrite NC films is around 80 $cm^2/(V\,s)$ with p-type behavior which is very high compared to other solution-processed electronic materials such as organic semiconductors or metal oxide semiconductors.

There are few methods to directly measure the carrier lifetime. Here we used a photoconductive response measurement that can reflect the density of defect states in the pyrite material. The presence of photoconductivity (photoresponse) is a prerequisite for a material to be a candidate for PV applications. Only high-purity pyrite shows a photoconductive response because defects such as metallic FeS will quench photoexcited carriers and eliminate the photoconductivity. In the past, photoconductivity has been barely observed at room temperature in both synthesized and natural pyrite crystals.[13,32] Here, in our studies, current voltage (I V) characteristics of a 400 nm thick FeS_2 film sandwiched between ITO and Al contacts in Figure 4A, show that the as-obtained pyrite FeS_2 NC film acts as a photoconductor, displaying a 12-fold increase in current under AM1.5 illumination in air at room temperature. The obvious and stable photoresponse showed in Figure 4B indicates the good quality and air stability of as-obtained pyrite FeS_2 NCs with fewer surface defect states, making an efficient solar cell device possible. There is no rectification behavior observed, and this indicates the absence of any Schottky barrier formed at the NCs/Al or NCs/ITO contacts. The fabrication of a pyrite FeS_2 solar cell device that incorporates metal oxide NCs to form p n junctions is underway.

In summary, we have synthesized uniform, phase pure, and air stable pyrite FeS_2 NCs, and the iron pyrite formation process was systemically studied. With the TOPO as a surfactant in the reaction mixture, we can produce pyrite FeS_2 NC films that show excellent stability in air. For those pyrite FeS_2 NCs synthesized

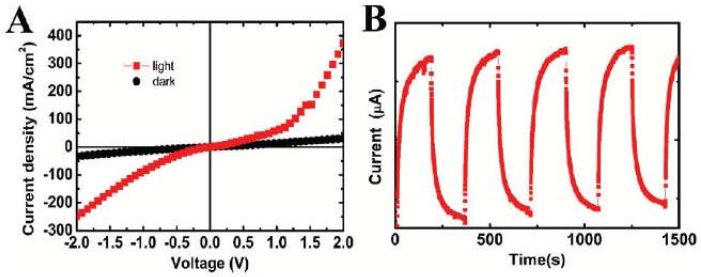

Figure 4. (A) $I-V$ measurement of ITO/400 nm FeS_2 NCs/Al device at dark and at AM 1.5 illumination. (B) Photo response of Al/FeS_2 400 nm/Al device with interlay of dark and AM1.5 illumination.

dx.doi.org/10.1021/nl202902z |Nano Lett. 2011, 11, 4953–4957

without TOPO, sulfur is easily released from the surface when they are exposed to air. This study shows that TOPO stabilizes the pyrite FeS_2 NCs surface in air by passivating both surface Fe and S sites. The pyrite NC films show excellent optoelectronic properties for efficient photovoltaic application.

' ASSOCIATED CONTENT

Supporting Information. Details of materials and experimental procedures, characterization of the reaction process by XRD, Raman spectra, and SEM, and characteration of the air stability of NC films. This material is available free of charge via the Internet at http://pubs.acs.org.

' AUTHOR INFORMATION

Corresponding Author
*E-mail: jhuang2@unl.edu.

' ACKNOWLEDGMENT

We thank Professor Yongfeng Lu for Raman spectra measurement and Professor Natale J. Ianno for the optical absorption and thickness measurement. Financial support by UNL layman awards is gratefully acknowledged.

' REFERENCES

(1) Wadia, C.; Alivisatos, A. P.; Kammen, D. M. *Environ. Sci. Technol.* **2009**, *43* (6), 2072–2077.
(2) Wadia, C.; Wu, Y.; Gul, S.; Volkman, S. K.; Guo, J. H.; Alivisatos, A. P. *Chem. Mater.* **2009**, *21* (13), 2568–2570.
(3) Altermatt, P. P.; Kiesewetter, T.; Ellmer, K.; Tributsch, H. *Sol. Energy Mater. Sol. Cells* **2002**, *71* (2), 181–195.
(4) Ennaoui, A.; Fiechter, S.; Pettenkofer, C.; Alonsovante, N.; Buker, K.; Bronold, M.; Hopfner, C.; Tributsch, H. *Sol. Energy Mater. Sol. Cells* **1993**, *29* (4), 289–370.
(5) Buker, K.; Alonsovante, N.; Tributsch, H. *J. Appl. Phys.* **1992**, *72* (12), 5721–5728.
(6) Ennaoui, A.; Fiechter, S.; Goslowsky, H.; Tributsch, H. *J. Electrochem. Soc.* **1985**, *132*, 1579.
(7) Ennaoui, A.; Fiechter, S.; Smestad, G.; Tributsch, H. *World Renewable Energy Congress. Energy and the Environment*; Pergamon Press: Oxford, 1990; p 458.
(8) Dasbach, R.; Willeke, G.; Blenk, O. *MRS Bull.* **1993**, *18* (10), 56–60.
(9) Murphy, R.; Strongin, D. R. *Surf. Sci. Rep.* **2009**, *64* (1), 1–45.
(10) Bouchard, R. J. *J. Cryst. Growth* **1962**, *2* (1), 40–44.
(11) Bausch, S.; Sailer, B.; Keppner, H.; Willeke, G.; Bucher, E.; Frommeyer, G. *Appl. Phys. Lett.* **1990**, *57* (1), 25–27.
(12) Puthussery, J.; Seefeld, S.; Berry, N.; Gibbs, M.; Law, M. *J. Am. Chem. Soc.* **2011**, *133*, 716–719.
(13) Yu, L.; Lany, S.; Kykyneshi, R.; Jieratum, V.; Ravichandran, R.; Pelatt, B.; Altschul, E.; Platt, H. A. S.; Wager, J. F.; Keszler, D. A.; Zunger, A. *Adv. Energy Mater.* **2011**, *1*, 748–753.
(14) Oertel, J.; Ellmer, K.; Bohne, W.; Rohrich, J.; Tributsch, H. *J. Cryst. Growth* **1999**, *198*, 1205–1210.
(15) Lin, Y.-Y.; Di-YanWang; Yen, H.-C.; Chen, H.-L.; Chen, C.-C.; Chen, C.-M.; Tang, C.-Y.; Chen, C.-W. *Nanotechnology* **2009**, *20*, 405207.
(16) Breier, J. A.; German, C. R.; White, S. N. *Geochem., Geophys., Geosyst.* **2009**, 10.
(17) Kleppe, A. K.; Jephcoat, A. P. *Mineral. Mag.* **2004**, *68* (3), 433–441.
(18) Turcotte, S. B.; Benner, R. E.; Riley, Andrew M.; Li, Jun; Wadsworth, Milton E.; Bodily, David *Appl. Opt.* **1993**, *32*, 935–948.
(19) Ferrer, I. J.; Nevskaia, D. M.; Delasheras, C.; Sanchez, C. *Solid State Commun.* **1990**, *74* (9), 913–916.
(20) Smestad, G.; Dasilva, A.; Tributsch, H.; Fiechter, S.; Kunst, M.; Meziani, N.; Birkholz, M. *Sol. Energy Mater.* **1989**, *18* (5), 299–313.
(21) Lalvani, S. B.; Weston, A.; Masden, J. T. *J. Mater. Sci.* **1990**, *25* (1A), 107–112.
(22) Smestad, G.; Ennaoui, A.; Fiechter, S.; Tributsch, H.; Hofmann, W. K.; Birkholz, M.; Kautek, W. *Sol. Energy Mater.* **1990**, *20* (3), 149–165.
(23) Golan, Y.; Patla, I.; Acharya, S.; Zeiri, L.; Israelachvili, J.; Efrima, S. *Nano Lett.* **2007**, *7* (6), 1459–1462.
(24) Hyun, B. R.; Zhong, Y. W.; Bartnik, A. C.; Sun, L. F.; Abruna, H. D.; Wise, F. W.; Goodreau, J. D.; Matthews, J. R.; Leslie, T. M.; Borrelli, N. F. *ACS Nano* **2008**, *2* (11), 2206–2212.
(25) Alivisatos, A. P.; Chan, E. M.; Mathies, R. A. *Nano Lett.* **2003**, *3* (2), 199–201.
(26) Li, X. F.; Wang, Y.; Meng, L. *Mater. Res. Bull.* **2009**, *44* (2), 462–467.
(27) Alivisatos, A. P.; Li, L. S.; Hu, J. T.; Yang, W. D. *Nano Lett.* **2001**, *1* (7), 349–351.
(28) Ellmer, K.; Tributsch, H. *Proc. Workshop Quantum Sol. Energy Convers. (QUANTSOL 2000), 12th* **2000**.
(29) Boughriet, A.; Figueiredo, R. S.; Laureyns, J.; Recourt, P. *J. Chem. Soc., Faraday Trans.* **1997**, *93* (17), 3209–3215.
(30) Hines, M. A.; Guyot-Sionnest, P. *J. Phys. Chem. B* **1998**, *102* (19), 3655–3657.
(31) Cotton, F. A.; Barnes, R. D.; Bannister, E. *J. Chem. Soc.* **1960**, No. May, 2199–2203.
(32) Fukui, T.; Miyadai, T.; Miyahara, S. *J. Phys. Soc. Jpn.* **1971**, *31* (4), 1277.